Residual strength and crack path predictions by the cohesive model

I. Scheider[1] and W. Brocks[1]

[1]Helmholtz Association of German Research Centres, GKSS Research Centre, 21502 Geesthacht, Germany, ingo.scheider@gkss.de

ABSTRACT.

The cohesive model for crack propagation analyses is incorporated into finite element programs by interface elements, which simulate the material separation. A drawback of these elements for the prediction of crack paths is that they are generated prior to the simulation and the number of possible directions for crack extension is limited. If there are only a few alternatives for the crack to extend, however, i.e. in bifurcation problems, interface elements can be profitably used for the numerical prediction of crack paths. Examples for this kind of problems will be given on both, the macroscopic and the microscopic scale. The former is the simulation of a stiffened cylindrical shell under internal pressure, where a skin crack may penetrate the rib or deviate. The latter is a unit-cell calculation for a fibre-reinforced material, where the fibre may debond or break.

INTRODUCTION

Cohesive models are used for numerical crack propagation analyses for several decades now. First introduced by Hillerborg et al. [1] in combination with finite element analyses, they have been used as interfaces, which represent the damage and failure properties of the material. As the crack can extend along the boundaries of solid elements only, the crack path is predefined by the mesh and no actual predictions are possible. Almost arbitrary crack path propagation can be achieved by introducing interface elements between all solid elements as a remedy. This issue has been investigated by several authors, e.g. [2,3,4,5], for many different classes of materials.

Even though there are other techniques better suited for arbitrary crack propagation, namely so-called embedded discontinuity models or X-FEM method [6] and the strong discontinuity approach [7], see also the review of Jirásek [8], there are still applications, where interface elements can be profitably used for the numerical prediction of crack paths. This is the case when there are only a few different possibilities for the crack to extend, i.e. in bifurcation problems on both, macroscopic and microscopic length scales. Crack-path bifurcation may be important in the frame of structural integrity analyses [9] or in micromechanical modelling, for example debonding or breaking of fibres in a

matrix [10, 11]. The present paper presents examples for both kinds of problems, which are solved using cohesive interface elements.

The applicability to predict the residual strength of components is demonstrated on a cylindrical shell with welded circumferential ribs under internal pressure, see Figure 1. If a crack exists that extends in longitudinal direction, the rib acts as a crack stopper. When the crack approaches the rib-to-skin connection, several possibilities for the crack exist to propagate further.
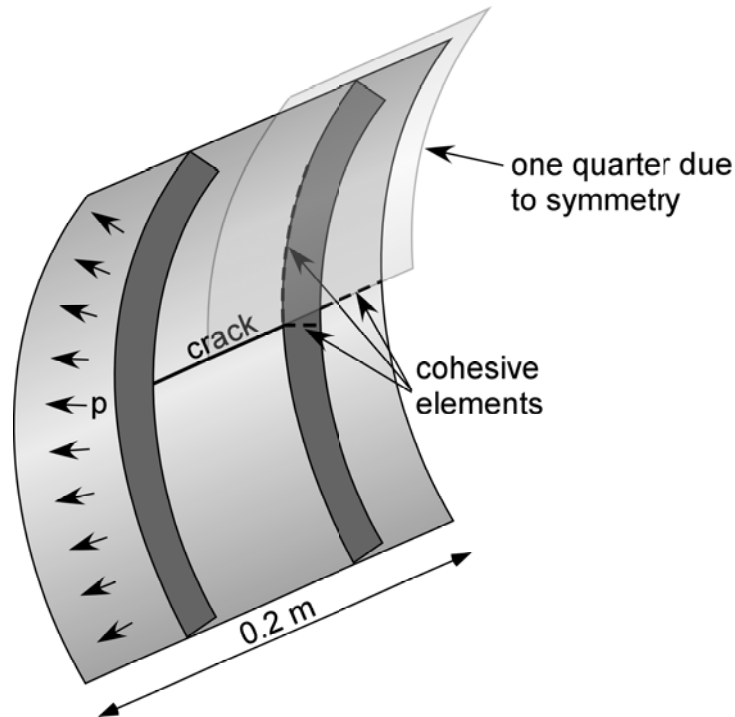

Figure 1: Cylindrical shell with welded circumferential ribs under internal pressure.

The second problem addressed in this paper, the debonding and breaking of fibres or particles in a composite material, is demonstrated by a simple axisymmetric unit cell calculation containing a single SiC fibre in a Ti-alloy matrix, see Figure 2. This material has already been investigated by Zeng et al. [12,13]. Though pure fibre fracture can be estimated by a tensile stress criterion [10], the cohesive model allows also for the interaction of breaking and debonding in complex loading configurations and arbitrary fibre orientations. The method can also be applied to compounds containing particle inclusions [14].
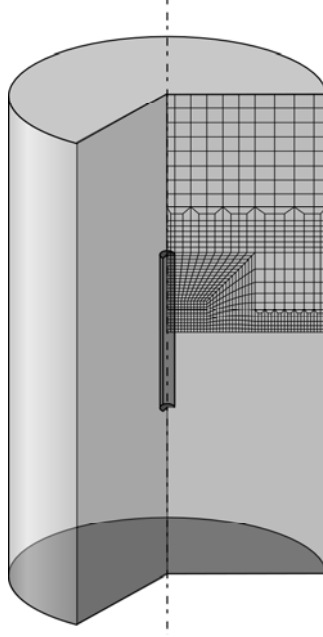
Figure 2: Axisymmetric unit cell of a fibre-reinforced material.

THE NUMERICAL MODEL

Cohesive models describe various kinds of decohesion processes by a relation between surface tractions or cohesive stresses, $\mathbf{T} = \{T_i\}$, $i = I, II, III$, having one normal, T_I, and two tangential (shear) components, T_{II}, T_{III}, in general, and the material separation, $\boldsymbol{\delta} = \mathbf{u}^+ - \mathbf{u}^- = \{\delta_i\}$. Various functions for the cohesive law, $\mathbf{T}(\boldsymbol{\delta})$, have been proposed in the literature, They have in common, that they contain two characteristic parameters per crack opening mode, namely a cohesive strength, $T_{i,0}$, and a critical separation, $\delta_{i,0}$. Alternatively, the work of separation,

$$\Gamma_{i,0} = \int_0^{\delta_{i,0}} T_i(\delta_j) d\delta_i \tag{1}$$

can be regarded as a material parameter instead of $\delta_{i,0}$. The parameters $T_{i,0}$ and $\delta_{i,0}$ or $\Gamma_{i,0}$ denote the characteristic parameters for pure mode I, II or III separations. For mixed mode situations, a coupling term has to be introduced. The constitutive behaviour of the cohesive model used throughout this paper has been proposed by Scheider et al. [5]. This model has been developed for fully coupled normal and tangential material separation based on a versatile traction-separation relation including irreversibility of damage at unloading. The general form writes

$$T_i = T_{i,0} f(\delta_i) g_i(\delta_j) \qquad (i, j = I, II, III \ , \quad i \neq j) \tag{2}$$

The function $f(\delta_i)$ in Eq. (2), which is the same for all three separation modes, determines the shape of the single-mode cohesive law, whereas $g_i(\delta_j)$ introduces the mode coupling, particularly between normal and shear separation. Using this approach, the shape of the single-mode cohesive law and the mixed-mode behaviour can be chosen independently. For three-dimensional simulations, it is reasonable to calculate the shear separation in one resultant tangential direction, only, since the separation behaviour should not depend on the finite element orientation. Only for shell structures, where all three separations denote different failure modes, the shear coupling is defined by

$$g_i(\delta_j) = \sqrt{g(\delta_k)g(\delta_l)} \qquad (i = I, II, III \, ; \, k = II, III, I \, ; \, l = III, I, II) \qquad (3)$$

The functions $f(\delta)$ and $g(\delta)$ are defined as follows:

$$f(\delta) = \begin{cases} 2\left(\dfrac{\delta}{\delta_1}\right) - \left(\dfrac{\delta}{\delta_1}\right)^2 & \delta < \delta_1 \\ 1 & \delta_1 < \delta < \delta_2 \, , \\ 2\left(\dfrac{\delta - \delta_2}{\delta_0 - \delta_2}\right)^3 - 3\left(\dfrac{\delta - \delta_2}{\delta_0 - \delta_2}\right)^2 + 1 & \delta_2 < \delta < \delta_0 \end{cases} \qquad (4)$$

containing two additional shape parameters, δ_1 and δ_2, and

$$g(\delta) = 2\left(\delta / \delta_0\right)^3 - 3\left(\delta / \delta_0\right)^2 + 1 \qquad (5)$$

The shape of these functions is shown in Figure 3. The single-mode cohesive law, eq. (4), is similar to the trapezoidal shape proposed by Tvergaard [15], but the present one is differentiable, and the mixture rule is different.
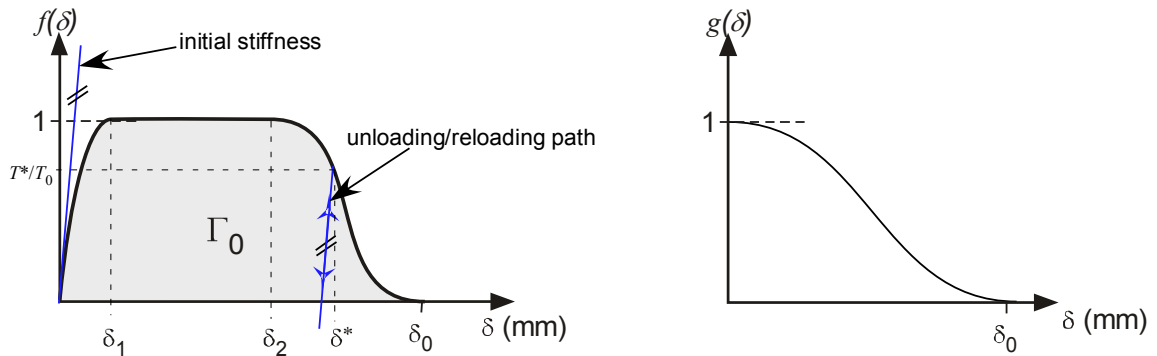

Figure 3. *Functions of the traction separation law used in Eq. (2).*

An additional convention is necessary for unloading and reloading. It is assumed, that the separation is irreversible as plastic deformation is and unloading and reloading follow a straight line according to the initial stiffness of the cohesive element as schematically shown in Figure 3. This performance is realised by a modification of the function f,

$$T_i = T_{i,0} f^*(\delta_i) g_i(\delta_j^*),$$ (6)

with

$$f^*(\delta_i) = \begin{cases} 2\left(\dfrac{\delta_i - \delta_i^*}{\delta_1}\right) + \dfrac{T_i^*}{T_{N,0}} & \text{for} \quad \delta_i \leq \delta_i^* \\ f(\delta_i) & \text{for} \quad \delta_i > \delta_i^* \end{cases},$$ (7)

where δ_i^* and T_i^* are the values of separation and cohesive stress reached before unloading. Compressive normal stresses should be accompanied by an infinite stiffness, which is numerically detrimental, so that the cohesive element is actually endowed with the initial stiffness under negative normal stresses. Shear separation can reverse its direction and follows the cohesive law after $|T_i| = |T_i^*|$.

STRUCTURAL APPLICATION

For complex and security relevant components it is necessary to prove the damage tolerance by several standard tests. One scenario for certification of new aircraft fuselage designs is the assumption of a two-bay crack. During this test, a section of the fuselage with several stringers and ribs containing a crack that reaches over two fields including a rib must be able to withstand the internal pressure occurring under high altitude flight conditions.

In an integral design of the fuselage, the stringers and ribs are joined to the skin by welding or adhesive bonding. The crack propagation depends strongly on the bonding quality, and one of the main questions is, whether the crack penetrates the rib or deviates and extends along it. The structure shown in Figure 1, is a simple model of an airplane fuselage containing a crack, which approaches a rib. Because of two existing symmetry planes, only a quarter section of the structure has been meshed with finite elements, see Figure 4. The structure is subject to monotonically increasing internal pressure. The crack can take one of three possible paths:

1. Continuing in axial direction along the panel and cutting the rib apart, resulting in two extending cracks.

2. Continuing in axial direction along the panel and debonding the rib from the panel along the weldment without cutting it, also leading to two crack tips.
3. Deviating by 90° to the original direction, cutting the skin along the rib without penetrating the latter, leading to a single crack, only.

In order to realise these three possibilities, four rows of cohesive elements are incorporated in the shell mesh, shown in Figure 4: Two at the symmetry plane, both at the skin (1) and at the rib (2), and two at the bond line between skin and rib (3 and 4). The locations of cohesive elements are shown together with their numbers in the detail sketch on the right of Figure 4. The cohesive elements may have different properties: the lines (1) and (3) represent material separation in the skin, the green line (2) the separation of the rib, the blue line (4) the fracture behaviour of the bonding between skin and rib, e.g. the laser weldment. Though the cohesive lines are displayed with a finite thickness in the sketch, they do not have any in the undeformed state, of course.
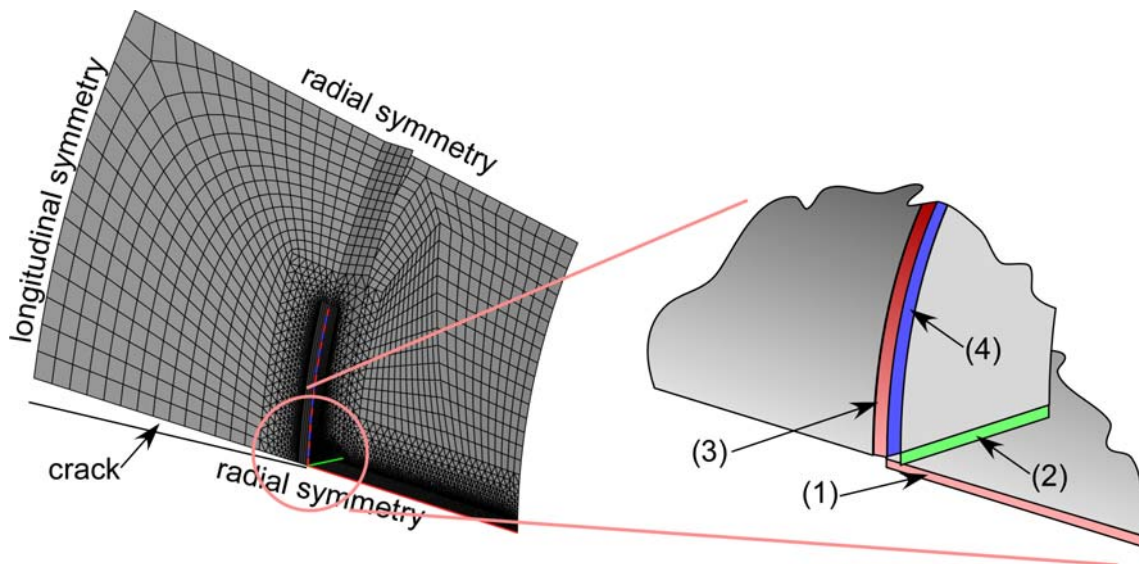

Figure 4. *Left: Finite element mesh of the structure shown in Figure 1. Right: Detail of the structure showing four rows of cohesive elements. (1) and (3) model separation of the skin, (2) separation of the rib, and (4) separation along the weldment.*

The present study is purely numerical, but properties of a real material have been used. They are taken from investigations performed by Nègre et al. [16,17,18], who studied an aluminium alloy of the 6000 series. It is assumed that skin and rib have the same properties, so that only two different parameter sets were to be used for the cohesive lines. The properties for the elastic-plastic behaviour and material separation are summarized in Table 1.

Table 1 *CaptionMaterial properties of the Aluminium and the weld zone.*

	Yield strength, σ_Y	Hardening exp., *n*	T_0 (MPa)	Γ_0 *(kJ/m²)*	δ_0 *(mm)*
Base material	300	0.672	550	20	0.073
Weld zone	200	0.248	407	8	0.039

Since the parameters were fixed based on the available experiments, the only parameter to vary is the geometry. Hence, the rib thickness has been varied for a fixed skin thickness (t_{skin} = 1 mm). It turned out that the crack remains in its original direction tearing the rib apart, if the rib thickness is chosen as 0.8 mm,. The pressure vs. crack tip opening displacement (CTOD) curve is shown in Figure 5. The crack extension at maximum pressure is shown in Figure 6 (left). If the rib thickness is increased to 1.3 mm, the maximum internal pressure can be significantly increased, and the crack is not able to penetrate the rib anymore, but deviates and fractures the skin adjacent to the rib connection, see the right picture in Figure 6. A further increase of the rib thickness does not have a big effect as also shown in Figure 5. For the cohesive parameters of the weldment that were taken from [18], the connection between rib and skin does not fail in any case.
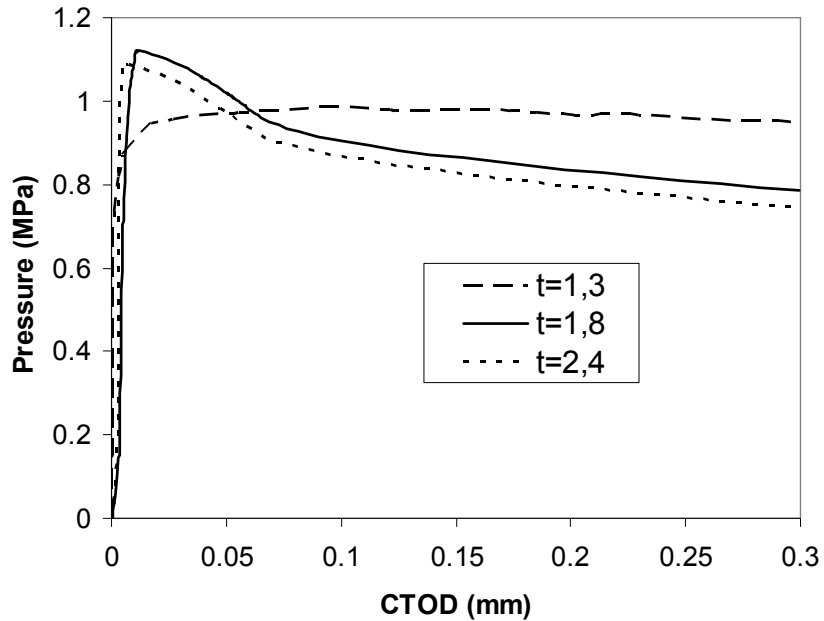

Figure 5: *Pressure vs. crack tip opening displacement (CTOD) showing the effect of rib thickness on the residual strength of the structure.*
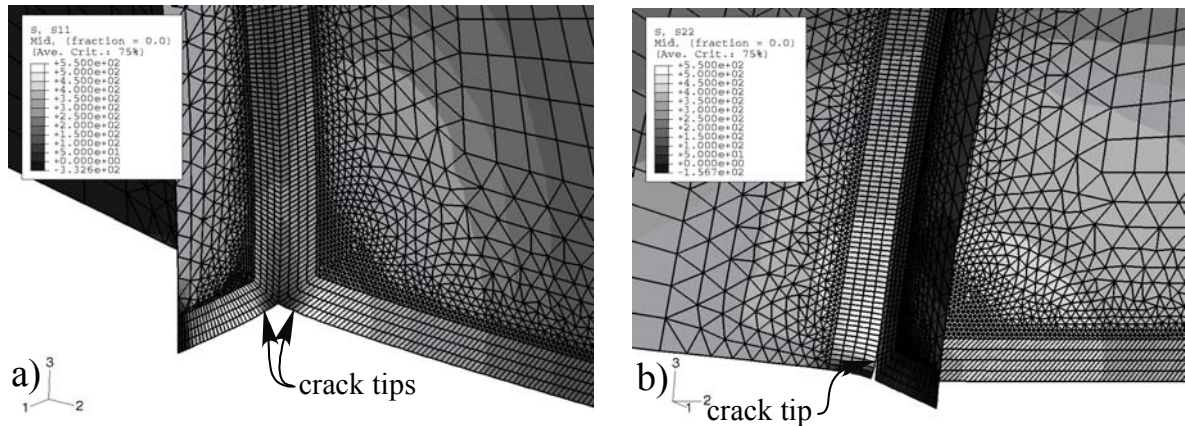
Figure 6: Detailed view of the crack extension at maximum load , effect of rib thickness on crack path. a) t_{rib} = 1.3 mm, b) t_{rib} = 1.8 mm

MICROMECHANICAL MODELLING

In fibre-reinforced materials with ductile matrix, the fibres improve the material's strength and fatigue behaviour. Intact fibres can bridge a crack extending in the matrix. Under quasi-static loading, the fibres can break or debond depending on their own strength and the strength of the interface [11]. The present study investigates a composite of a Ti-6 Al-4 V matrix with SiC fibres [12]. Assuming a periodoic microstructure, a representative volume element (or unit cell) consisting of a single fibre with a length of 1 mm and a radius r_f = 50 µm in a surrounding matrix (radius R = 1 mm) is modelled, as shown in Figure 2. The respective fibre-volume fraction is f_f = 8.33E-04. In a first step the unit cell is cooled down in order to obtain a compressive stress at the interface due to mismatch of thermal expansion. Afterwards, uniaxial tension is applied to simulate crack extension in the matrix with subsequent fibre breaking or debonding. Cohesive elements are introduced around the fibre and at the symmetry line, both in the fibre and in the matrix. An initial circumferential crack is introduced in the matrix. The temperature dependent material properties for the matrix and the fibre are taken from [12]. The cohesive properties for the different material separations are summarized in Table 2. These values are partly also taken from [13], the others are reasonable values for this material.

Table 2: Cohesive properties of the fibre, the matrix and the matrix-fibre-interface

	T_0 (MPa)	Γ_0 (J/m²)	δ_0 (mm)
Fibre debonding (tangential)	450	0.25	0.001
Fibre debonding (normal)	1000	0.55	0.001
Fibre breaking (normal)	4450	2.45	0.001
matrix cracking	1100	12.10	0.02

It turns out that the fibre breaks long before the cohesive strength in tangential direction at the interface between fibre and matrix is reached. Even if the normal fibre debonding strength, which is the significant parameter at the top of the fibre, is set to a rather low value and therefore the fibre head debonds first, the tangential cohesive stress is sufficient to prevent debonding before the fibre breaks. This behaviour does not only depend on the cohesive properties for debonding and breaking, but also on the ratio of radius and length of the fibre. Of course, a longer fibre is more susceptible to breaking, since the area where the tangential stress acts, is longer. Equilibrium requires

$$2\pi r_\mathrm{f} \int_0^{l_\mathrm{f}/2} \sigma_{rz}^{\mathrm{inter}} dz + 2\pi \int_0^{r_\mathrm{f}} \sigma_{zz}^{\mathrm{fibre}} r dr + 2\pi \int_0^{r_\mathrm{f}} \sigma_{zz}^{\mathrm{inter}} r dr = 0 \,, \tag{8}$$

and as a first estimate assuming homogeneous stresses, the sufficient condition for debonding requires

$$\frac{r_\mathrm{f}}{l_\mathrm{f}} > \frac{T_{\mathrm{II},0}^{\mathrm{debond}}}{T_{\mathrm{I},0}^{\mathrm{break}} - T_{\mathrm{I},0}^{\mathrm{debond}}} \,, \tag{9}$$

For a length of $l_\mathrm{f} = 1$ mm, the critical fibre radius is $r_\mathrm{f} = 130$ μm. Due to inhomogeneous stress distribution, debonding actually occurs for lower values, already, as the following study on the effect of the fibre geometry shows, where different fibre radii, namely $r_\mathrm{f} = 60, 75, 100$ and 150 μm, with respective fibre-volume fractions of $f_\mathrm{f} = 1.2\mathrm{E}{-03}, 1.875\mathrm{E}{-03}, 3.33\mathrm{E}{-03}$ and $7.5\mathrm{E}{-03}$ have been simulated.

For a fibre radius of 60 μm, the fiber debonds partly before it finally breaks. For $r_\mathrm{f} = 75$ μm, the maximum normal stress reached in the fiber is 4160 MPa, which is lower than the cohesive strength, so that debonding occurs. The respective curves of normalised load, F/F_Y, vs. mesoscopic strain $E = \Delta l/l_0$, are shown in Figure 7. The load drops, visible for all but the smallest fibre, are due to debonding of the fibre head. A significant effect of fiber-head debonding on the residual strength of the RVE occurs for $r_\mathrm{f} = 150$ μm.
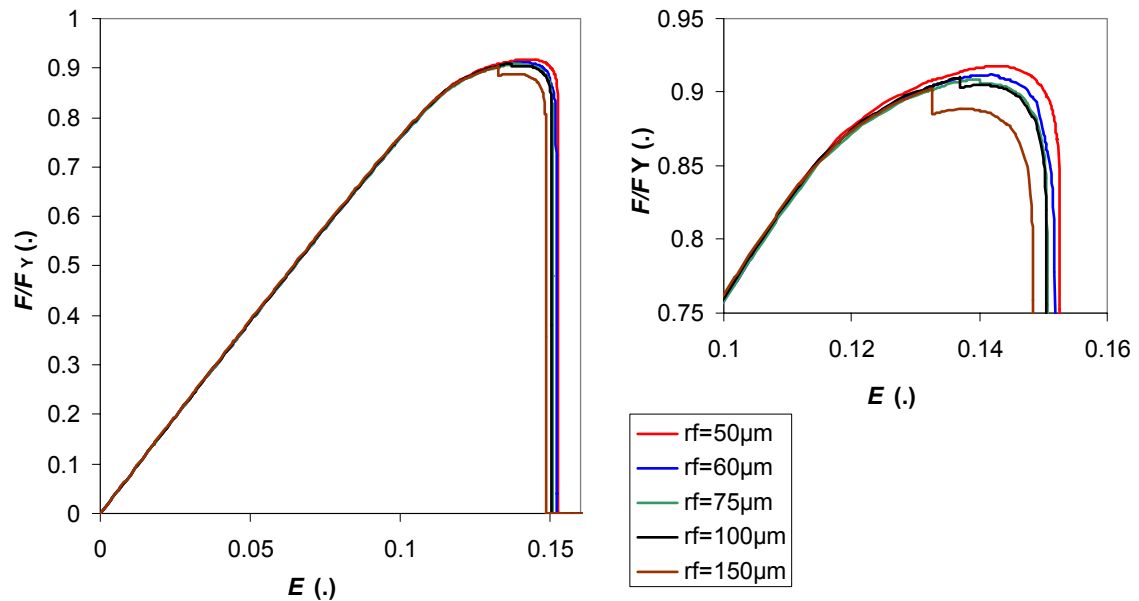
Figure 7: Load-displacement curves for the metal-matrix composite with varying fibre radius.

CONCLUSIONS

It has been shown that the cohesive model can be used to predict the path of a crack approaching a discontinuity and having a limited number of possibilities for further extension. This discontinuity can be a geometrical one like a stiffener or a changing plate thickness, or a material one like a phase boundary. In such cases bifurcation problems arise, where the crack may either keep its original direction or deviate and extend along the discontinuity.

Two examples have been presented. On the structural (macro) scale, cohesive interface elements have been applied to determine whether a crack in a stiffened structure deviates at the connection between skin and stiffener. On the microscale an axisymmetric unit cell containing a single elastic fibre in a ductile matrix under combined thermal and tensile loading has been investigated. Inserting cohesive elements at the interfaces and along the radial symmetry line in the centre of the fiber, it could be predicted when the fibre breaks and when it debonds.

The examples demonstrate that cohesive elements are useful tools for crack path predictions even though the crack extension is limited to predefined paths. The general advantages of the cohesive model compared to others such as microstructural based damage and embedded discontinuity models, in particular its versatile applicability, the robustness of the simulations and the efficiency for large crack extension, can be exploited for all of these cases.

REFERENCES

1. Hillerborg, A., Modeer, M., Petersson, P.E. (1976) *Cement Concrete Res.* **6**, 773-782.
2. Xu, X.-P., Needleman, A. (1994) *J. Mech. Phys. Solids* **42**, 1397-1434.
3. Tijssens, M.G.A., van der Giessen, E., Sluys, L.J. (2000), *Mech. of Mater.* **32**, 19-35.
4. Zavattieri, P.D., Raghuram, P.V., Espinosa, H.D. (2001) *J. Mech. Phys. Solids* **49**, 27-68.
5. Scheider, I., Brocks, W. (2003) *Eng. Fract. Mech.* **70**, 1943-1962.
6. Moës, N., Belytschko, T. (2002) *Eng. Fract. Mech.* **69**, 813-834.
7. Simo, J.C., Oliver, J. (1994). In: *Fracture and Damage in Quasibrittle Structures*, pp. 25-39, Z.P. Bazant et al. (Eds.), E. and F.N. Spon, London.
8. Jirásek, M. (2000) *Comput. Methods Appl. Mech. Engrg.* **188**, 307-330.
9. Scheider, I., Brocks, W. (2005). In: *Proc. 5th Int. Conf. on Comp. Shell and Spatial Struct.*, Ramm, E. et al. (Eds.).
10. Tvergaard, V (2004), *Mater. Sci. Engng. A* **369**, 192-200.
11. Evans, A.G. (1991), *Mater. Sci. Engng. A* **143,** 63-76.
12. Zeng, W.D., Peters, P.W.M., Tanaka, Y. (2002) *Composites: Part A* **33**, 1159-1170.
13. Peters, P.W.M., Hemptenmacher, J., Zeng, W.D. (2006). In: 38. Tagung DVM-Arbeitskreis Bruchvorgänge, pp. 207-223, M. Kuna (Ed.), DVM Berlin (in German)
14. Steglich, D., Siegmund, T., Brocks, W. (1999) *Comp. Mat. Sci.* **16**, 404-413.
15. Tvergaard, V., Hutchinson, J.W. (1992) *Int. J. Solids Struct.* **31**, 823-833.
16. Nègre, P., Steglich, D., Brocks, W. (2005) *Int. J. Fract.* **134**, 209-229.
17. Nègre, P. (2006) Damage and fracture mechanisms investigations of an aluminium laser beam weld, Dissertation, TU Hamburg-Harburg.
18. Scheider, I., Nègre, P., Brocks, W. (2006). In: 38. Tagung DVM-Arbeitskreis Bruchvorgänge, pp. 207-223, M. Kuna (Ed.), DVM Berlin (in German)